Eur. Phys. J. Special Topics **226**, 3315–3324 (2017)

DOI: 10.1140/epjst/e2016-60345-4

THE EUROPEAN PHYSICAL JOURNAL SPECIAL TOPICS

Regular Article

Basins of attraction in human balance

Victoria A. Smith[a], Thurmon E. Lockhart, and Mark L. Spano

School of Biological and Health Systems Engineering, Arizona State University, Tempe, AZ 85281, USA

Received 25 October 2016 / Received in final form 14 February 2017
Published online 28 December 2017

Abstract. Falls are a recognized risk factor for unintentional injuries among older adults, accounting for a large proportion of fractures, emergency department visits, and urgent hospitalizations. Human balance and gait research traditionally uses linear or qualitative tests to assess and describe human motion; however, human motion is neither a simple nor a linear process. The objective of this research is to identify and to learn more about what factors affect balance using nonlinear dynamical techniques, such as basin boundaries. Human balance data was collected using dual force plates for leans using only ankle movements as well as for unrestricted leans. Algorithms to describe the basin boundary were created and compared based on how well each method encloses the experimental data points as well as captures the differences between the two leaning conditions.

1 Introduction

As a risk factor for unintentional injuries among older adults, falls account for a large proportion of fractures, emergency department visits, and urgent hospitalizations [1] and are the leading causes of disability in older adults. According to the CDC's Web-based Injury Statistics Query and Reporting (WISQARS) [2], in 2010, 3.7 million people over the age of 50 reported non-fatal fall-related injuries. Every year, almost a third of people over the age of 65 fall at least once and 10–15% of those falls cause serious injuries or death [3]. Early prevention and intervention can reduce the number of falls [4]. We want to identify at-risk fallers before the first fall in order to reduce the overall number of falls and thus the number of injuries that occur due to a fall.

Maintaining an upright posture is a complex sensorimotor control system involving visual, vestibular, and proprioceptive systems [5]. The integration of all of these inputs allows people to balance, walk, and go about their daily lives without having to concentrate on the movements themselves. Without correct integration, or if an individual system starts to fail or degrade, performing those simple daily motions becomes difficult and can lead to falls. Fall risk factors are often viewed only with linear measures through tests like Timed Up and Go, Tinetti's mobility index and others which look at the time taken to walk a given distance, walking velocity, and sway area among other parameters [6,7]. These types of tests are very simple diagnostics and are easily calculable or are strictly qualitative in nature. Some of the

[a] e-mail: vasmith5@asu.edu

more promising predictors of fall risk have sprouted from analyzing stability with nonlinear dynamical tools such as Lyapunov exponents [8,9], stochastic resonance [10], and entropy [11–13]. These postural stability metrics are capable of identifying the differences between individuals who have a history of falling, "fallers", and those who do not have a history of falling, "non-fallers" [14–16]. Despite being able to identify these individuals *after* they have fallen, use of these measures as clinical indicators is ambiguous [17]. A more complex algorithm or model may better describe the observed innate motion in order to separate individuals that have a normal and stable stance from individuals who are unstable and at risk of falling.

Currently there are very few models that attempt to describe human postural stability or the ability to remain standing even when an individual's posture is perturbed. One of the more promising models, by Stirling and Zakynthinaki [18], describes postural stability as a dynamical system that has a basin of attraction. In essence, the upright standing position is a stable attractor and balance is maintained as long as the body's position remains within the basin of attraction. If the body moves outside of this basin an individual will lose their balance and fall or require a reactionary response in order to stop from falling. Note that Stirling and Zakynthinaki did not create a true phase space, which requires position and momentum, but only use a portion of the phase space by using calculated lean angles. We will be adapting our definition of the phase space to their interpretation from this point forward.

Here we build upon the aforementioned method and compare the different methods for creating basin of stability models. In Section 2 of this paper we discuss the protocols used to collect data that were used for comparing all of the models. Section 3 describes the methods used to create the different basin models, including the 2004 Zakynthinaki model, basic ellipses, two point ellipses, convex hulls, and singular value decomposition. Sections 4 and 5 of this paper discuss and compare the results from each method. The purpose of this paper is to develop algorithms and test methods that have practical clinical applications to future work.

2 Experimental procedures

Our procedure was adapted from Zakynthinaki et al. [19]. The experiment consisted of leaning in eight distinct directions, where the subject's initial and final position was standing upright on a force plate with both feet together on the floor and with hands on their hips. The subject was asked to lean as far and as fast as he could from this initial position in eight cardinal directions: forward, backward, left, right, forward-left, forward-right, backward-left, and backward-right. The trial was deemed successful if the subject was able to regain his balance and return to the initial position. This was done for two different leaning conditions: rigid body, allowing for movement only at the ankles, and non-rigid body, allowing the subject to use all of his lower extremity joints at the subject's discretion. The difference in the leaning styles is illustrated in Figure 1. Three trials for each direction were taken, the order of all 28 leans was randomized before the experiment started. Additionally, the subject was asked to stand still for 30 s, quiet stance, at three separate times during the experiment, after every eight leans. In order to avoid fatigue, the subject was asked to come back at a later time to perform the other leaning condition.

Our subject was a healthy, 28-year-old male. A GRAIL: Gait Real-time Analysis Interactive Lab, from Motek Medical was used to collect data. This system contains two force plates (Bertec), 10 motion analysis cameras (Bonita), and software which captures reflective marker position and force plate data. Ground reaction forces were collected using dual force plates (Bertec) at 1000 Hz. The ground reaction forces were filtered using a low-pass 4th order Butterworth filter at 7 Hz.

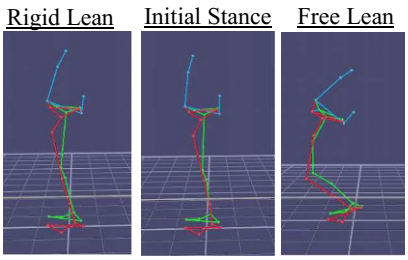

Fig. 1. Comparison of lean types with respect to the initial stance. The subject was asked to lean backwards under the rigid and free conditions.

3 Basin boundary models

3.1 General description

The importance of building several models included trying to find the best fit to describe the basin of stability and to quantify the primary directions, symmetry, and shape of the leans. In all of the models, we assume that the initial position of the subject is the vertical position of quiet stance and that the initial perturbation is away from the vertical.

The angles, θ_x and θ_y, are the movements in the x (anteroposterior or front–back) and y (mediolateral or left–right) directions, respectively, in relation to the filtered ground reaction forces recorded from the force plate. In the original paper [18] only a single force plate was used to calculate these angles. In order to simulate the effect of having only a single force plate from a dual force plate system the following equations were adapted:

$$\theta_x = \tan^{-1}\left(\frac{F_{x1}+F_{x2}}{F_{z1}+F_{z2}}\right), \quad \theta_y = \tan^{-1}\left(\frac{F_{y1}+F_{y2}}{F_{z1}+F_{z2}}\right). \tag{1}$$

Using this notation, F_z is the vertical component of the ground reaction force and F_x, F_y are the components of the resultant force in the anteroposterior and mediolateral directions, respectively. The force plate under the left foot and right foot are designated force plate 1 and 2, respectively.

The upright attractor in the phase space, i.e. the vertical state, corresponds to the condition that $\theta_x = \theta_y = 0$. The phase space of θ_x and θ_y includes a region, bounded by the "critical curve", where upright balance is maintained. If the body is perturbed beyond this curve, it will be attracted to the "fallen" attractor and must either take a step to regain balance or fall. For simplicity, all equations used to describe these methods will refer to θ_x as x and θ_y as y.

3.2 Foundation model (2004 Zakynthinaki method)

In their 2004 paper, Stirling and Zakynthinaki [18] developed an equation:

$$Ax^2 + Bx + Cy^2 + Dy + Gxy^2 + Hx^2y + Ix^2y^2 + Jxy - E = 0, \tag{2}$$

to describe the critical curve or *basin of stability boundary*. The constants (A–J) are derived from the maximum lean angles in the forward, back, left, and right directions,

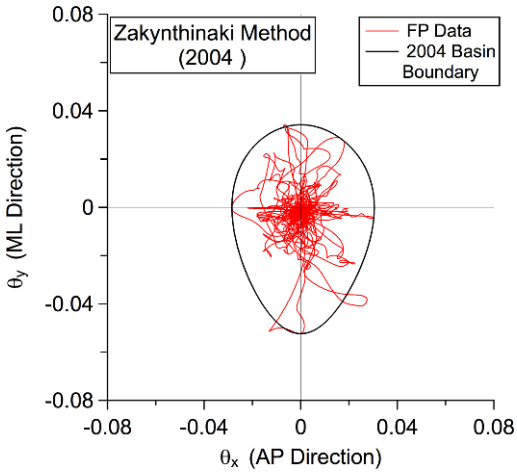

Fig. 2. Phase space of rigid lean data. The solid black line denotes the 2004 Zakynthinaki fit. It is important to note that the data uses only one lean in each of the 8 directions to make this plot and not all 24 leans collected. The force plate (FP) data for the other backward and forward leans violated the assumptions of the Zakynthinaki model due to the fact that the backwards leans were farther than the forward leans. All of the units in this plot and all of the following plots are in radians.

and I is a scaling factor and was chosen to be 0.3. This equation makes three assumptions. First, the values of the maximum left and backward leans must be less than zero and the maximum right and forward leans must be greater than zero. Second, the maximum forward lean angle must be greater than the maximum backward lean angle. Third, maximum leans in the left and right directions are approximately equal. Figure 2 applies it to our data and it is discussed further in Sections 4 and 5.

3.3 Basic Ellipse (BE) fit

The first two algorithms are based on the equation of an ellipse:

$$1 = \frac{[(x-h)\cos(\phi) + (y-k)\sin(\phi)]^2}{a^2} + \frac{[(x-h)\cos(\phi) - (y-k)\sin(\phi)]^2}{b^2}, \qquad (3)$$

where (h, k) is the center of the ellipse, a and b are the lengths of the semi-axes, and ϕ is the angle at which the ellipse is tilted with respect to the x-axis. Let λ=$(x-h)\cos(\phi)$+$(y-k)\sin(\phi)$, η=$(x-h)\cos(\phi)$−$(y-k)\sin(\phi)$ such that equation becomes $1 = \frac{\lambda^2}{a^2} + \frac{\eta^2}{b^2}$ easily recognized as an ellipse.

To determine the angle, ϕ, the least squares regression line of a session's lean data was calculated. The tilt angle is the inverse tangent of the slope of the regression line, equation (4). This angle is based purely on the experimental data and is the same angle regardless of which algorithm is being used:

$$\phi = \tan^{-1}(\text{slope}). \qquad (4)$$

An ellipse was chosen as the first approximation of the basin of stability from the experimental data.

The first algorithm, Basic Ellipse fit, creates the simplest ellipse based on the data. The center point is defined as the midpoint between the maximum and minimum values of x and y, where the semi-axes of the ellipse were defined as the difference between the center point of the ellipse and the maximum x and y points, equation (5), respectively:

$$h = \frac{x_{\max} + x_{\min}}{2}, \quad k = \frac{y_{\max} + y_{\min}}{2}, \quad a = x_{\max} - h, \quad b = y_{\max} - k. \tag{5}$$

This algorithm is very fast and simple, which is ideal if this data is to be processed on a handheld device for clinicians to use. The primary issue is that not all of the data lie within the BE basin boundary. The basin boundary should be the divide between a region where an individual can recover from a perturbation and a region where an individual is unable to recover.

3.4 Two-Point Ellipse (TPE) fit

The Two-Point Ellipse algorithm creates an ellipse knowing two points that must lie on the boundary line. The algorithm chooses two of the four maximum lean angles by minimizing how many data points fall outside of the boundary. Two of the maximum lean angles are used at a time to determine both the major and minor semi-axes' lengths and every permutation of the four maximum lean angle coordinates is used. The least number of points that fall outside of the drawn ellipse determines the best ellipse fit. For each pair of coordinates, λ and η are calculated as described in the following equation using two points on the ellipse, the center point, and the tilt angle. The semi-axes calculated analytically using the following equations:

$$a^2 = \lambda_1^2 / \left[1 - \frac{(\lambda_2 \lambda_1)\,\eta_1^2 - \eta_1^2}{\left(\frac{\lambda_2}{\lambda_1}\right)\eta_1^2 - \eta_2^2} \right], \quad b^2 = \frac{\left(\frac{\lambda_2}{\lambda_1}\right)\eta_1^2 - \eta_1^2}{\left(\frac{\lambda_2}{\lambda_1}\right) - 1}. \tag{6}$$

This algorithm includes 99.98% of data points, but lost the ability to describe the shape of the data, as seen in Figure 3. The area of the basin is much greater than the BE algorithm. This algorithm is more complicated than the BE fit but would still be able to run on a simple device for clinical use.

3.5 Convex Hull (CH) fit

To ensure that no data point could lie outside of the basin boundary, we used convex hulls. A *Convex Hull* is the smallest convex curve containing all of the points in a given set [20]. The algorithm used in this paper was based on the Graham scan [21] which has a worst case run time of $O(n \log n)$. The algorithm finds the "extreme" or outermost points in the given coordinate dataset that can completely encapsulate the data by creating a n-sided polygon. Figure 4 shows the Convex Hull for rigid and free leans. References [20–22] provide a detailed explanation of the Convex Hull algorithm.

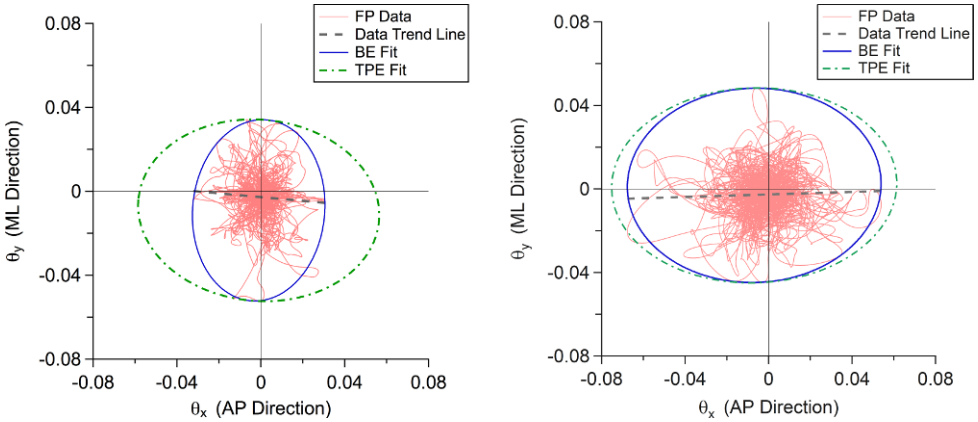

Fig. 3. Basic Ellipse and Two Point Ellipse comparison. BE is the solid blue line and TPE fit is depicted by the dashed green. The rigid (left) and free (right) lean data are compared. Data is not completely included within the basin fit for either lean.

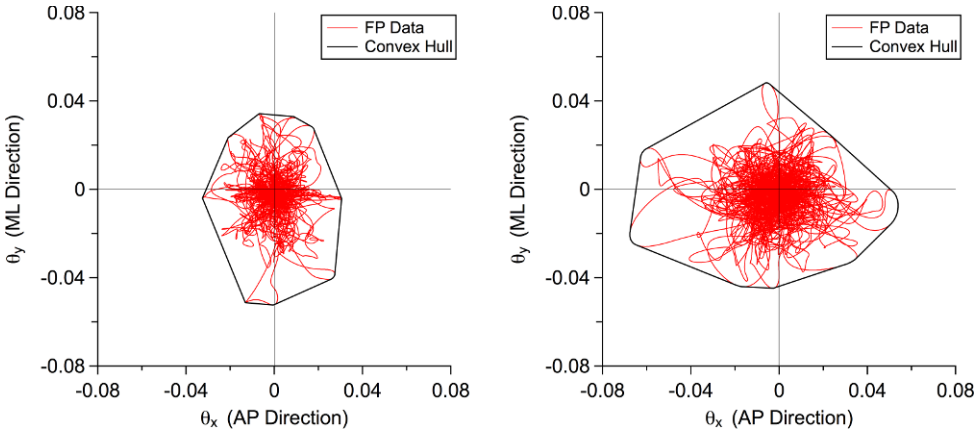

Fig. 4. A *Convex Hull* fit ensures that all data points are included within the resulting polygon. This method uses the minimum number of outside points to make the final shape.

4 Experimental results

Figure 2 shows the 2004 Zakynthinaki method for calculating a basin boundary using rigid lean data. A critical curve could not be generated by their method for the free lean data because it violates the assumption that a person does not lean farther backwards than forwards.

Figures 3 and 4 compare the Basic Ellipse (BE) fit, Two Point Ellipse (TPE) fit, and Convex Hull (CH) fit methods to generate a basin of stability for rigid and free leans, respectively. The percent difference between the mediolateral (left to right) and anteroposterior (front to back) ranges of free and rigid leans are 7.19% and 63.50%, respectively.

In Figure 3, the BE fit does not enclose the data for either lean type. When the data is closely spaced, e.g. rigid lean data, the fit does well in not having excess white space but when there are far excursions from the center more white space is inevitably included to capture the movement. The TPE fit was able to include more of the data inside its basin boundary; however, it loses the true shape of the data.

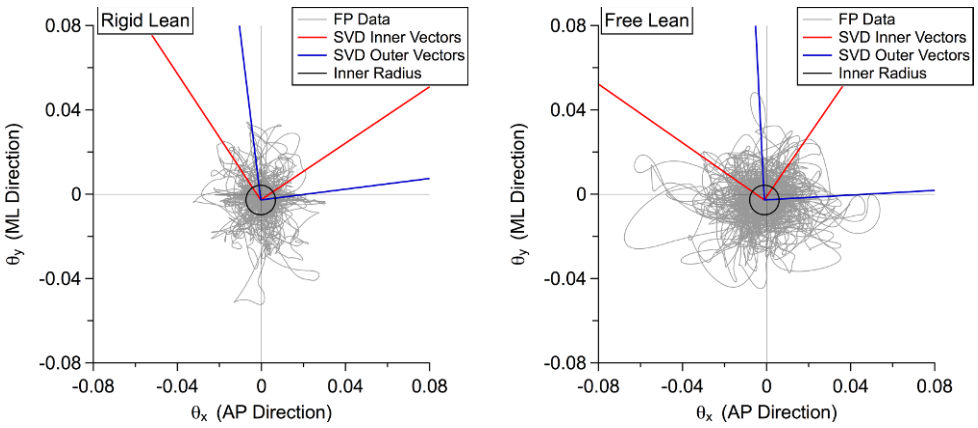

Fig. 5. Principle vectors calculated for rigid (left) and free (right) leans using SVD. The inner radius (black) is 0.007 radians and defines the inner and outer regions. The center of mass of the data for the rigid and free leans was calculated to be (−0.0004, −0.0027) and (−0.0011, −0.0026), respectively.

The regression trend line (blue) is used as a tilt calculation for both ellipses but does not represent the ellipse semiaxes.

All of the fits improved on enclosing more points within the basin of stability; however, the area and perimeter also increased, most markedly with the TPE fit. The CH approach kept the area the smallest and closest to the original algorithm while the BE fit had the smallest perimeter. The TPE had the best inclusion of the data, excluding the Convex Hull; however, the area and perimeter are much larger than the 2004 Zakynthinaki method. The CH fit maintains the integrity of the shape and symmetry of the data and encloses every data point, improving upon all of the previous models.

All of the preceding algorithms either fail to provide information on the primary directions of the leans or, in the case of the ellipse fits, provide information based mostly on outer points rather than the entire data set. *Singular value decomposition* (SVD) [26,27] derives the primary directions from the data. From quiet stance data, normal sway radius was determined to be 0.007 radians, here taken as the boundary between small (inner points) and large (outer points) excursions. SVD was applied (Fig. 5) separately to the inner and outer data points to distinguish the different characteristics of small versus large posture angles, see Figure 5. Note that there are significant differences between the primary directions for small versus large angles, further characterizing sway and by inference balance control.

5 Discussion

The objective of this research was to develop algorithms for finding the basin of stability from experimental data. The importance of building several models was trifold. First, we wanted to find the best fit to describe the basin of stability; second, to quantify the different characteristics that define each lean type; and lastly, develop an algorithm that could be run without arbitrary user input for a better translation into a clinical setting. We collected force plate data for two lean conditions, a free lean where no other instructions other than the direction of leaning was given and a rigid lean where only ankle movements were allowed. This rigid lean type is what is usually seen in the literature [24,25] but it is not a very natural motion. Initially

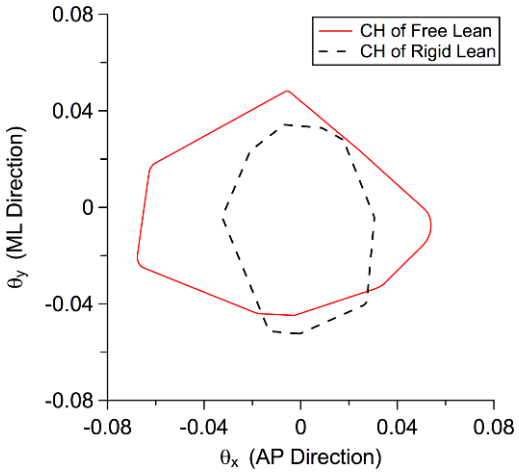

Fig. 6. Convex Hull comparison of rigid (black) and free (red) leans. Force data from rigid and free leans, not shown, are used to calculate these convex hulls. This plot compares the different size and shape of the convex hulls with respect to the rigid and free leans.

researchers used this style because it reduces the degrees of freedom making it easier to do certain calculations as well as reduces possible confounding factors. We included a free lean motion to see how much information about a person's balance is lost when using a rigid lean.

The differences between the two lean types can be seen when you compare them on the same plot in Figure 6. It is evident that the range of mediolateral leans is similar while the anteroposterior leans are distinctly different. In the free lean data there is only a 7% difference between leaning backwards and forwards, which is less than we expected. While this subject could possibly be more skilled at leaning back than the normal population, the successful act of leaning backwards and returning to a standing position involves more joints, i.e. hips, knees, and ankles, than leaning forward. When asked to lean forward as far as possible most people bend at the waist, not shifting the center of mass very far, and then try to lean further by going up on their toes, which actually shifts the center of mass. It is also possible that humans have more control leaning forward because it is done naturally in some normal daily activities, such as bending over and picking something off the ground, whereas leaning backwards is an unusual motion unless you are trying to recover from a fall.

Each of the methods we developed – BE fit, TPE fit, and CH fit – included more of the data compared to the Zakynthinaki model. The ellipse algorithms do improve in inclusion, but some lose the ability to adequately describe the overall shape of the data. The CH fit was the best algorithm of the new basin of stability methods. It was able to encapsulate all points as well as maintain the integrity of the shape of the data. One important point to make about the shape of the overall basin of stability is that we do not know how close to the data the basin of stability should be because it is impossible to collect information about every location within this phase space.

We previously defined the basin of stability to mean that all the points that are enclosed within that region will converge back onto the center attractor. If an individual moves beyond the boundary, then they are now in a state of falling or must act in order to recover to the standing position. The 2004 Zakynthinaki method was unable to encompass all of the data points; however their later methods were able to enclose all of the points but required "special" points for making the final basin of stability. These newer methods are more computationally expensive to reproduce

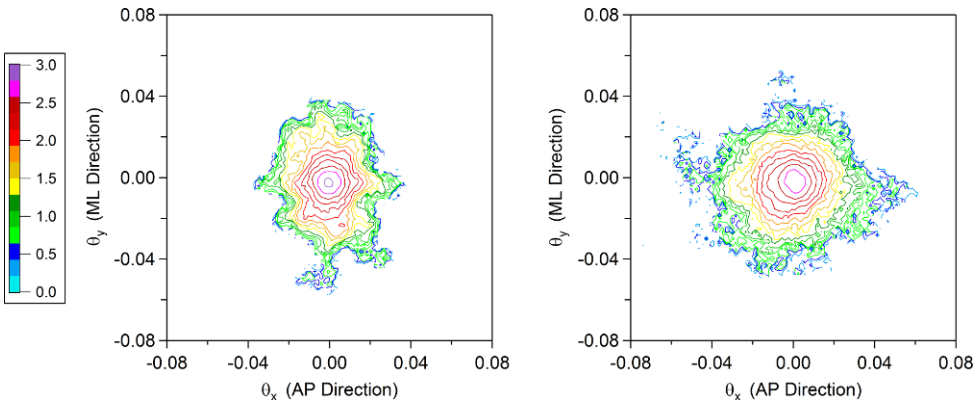

Fig. 7. Dwell time maps for rigid (left) and free (right) leans. Each plot includes all 24 unfiltered leans collected for the given condition. The color scale represents the log of the number of points in each box.

and would not be ideal for a clinical test. Therefore we only compared to their 2004 method and developed methods of encapsulation that do not require handpicked points and that allow the collected data to be processed quickly for clinical use.

Traditionally, a phase space is a plot comparing positions and momenta. However, what we have called a phase space thus far compares the position in the anteroposterior direction to the position in the mediolateral direction. Since we have two positions, a correct phase space should have momenta in each direction as well, thus creating a 4-dimensional space. In order to come closer to producing a proper phase space, we relate each position to the magnitude of the velocity by calculating information density (Fig. 7).

Information density was calculated by dividing the x- and y-axes into a grid of 100 by 100 boxes, with a box height and width of 0.0016 radians. The number of data points located in each box was counted and corresponds to the density of information in a given box. The log of the density in each box is displayed in Figure 7. We called this a *dwell time plot*. The larger the number of points in a given box, the greater the density and correspondingly the longer the subject spent in that position (dwell time). As the color moves from the reds to the blues, the subject spends less time in that region, passing through any given box more quickly, thus implying a larger velocity (which is proportional to the momentum).

Figure 7 depicts the dwell time map for each unfiltered lean. The shapes of the two plots are very different. The outline of the leaning direction can be seen in the rigid map while the free lean map has no directional distinctions. This could indicate that the physical restriction of locking the ankles increases the difficulty level for the subject to control their movements, so the subject moves slowly and carefully to lean as far as possible before returning to the initial position.

Both maps gradually transition from denser at the center to less dense outer areas. The rigid lean has a higher density of points at the center of the map. At the fringes, the free lean map has more blue. While the blue color indicates less time spent in that box, when integrated over the total number of blue boxes, it is apparent that more time was spent at that *radius*. Thus it can be inferred that the free movements were slower, and presumably more controlled, at that distance from the initial position.

In the future, the lean transitions will be quantified by calculating the joint torques and power, in order to estimate the energy required during each phase of a lean. In addition to the force plate data, three-dimensional position data for 25 reflective markers placed at key anatomical features was recorded and will be used for these

energy calculations. It is hoped that this will help distinguish differences between different age groups and may help to identify people at risk for falling.

It is hoped that the application of basins of attraction to postural stability may help quantify previously subjective clinical measures. The intent is to use these algorithms to create a *quantitative* fall risk assessment tool to test different populations including healthy young, healthy elderly, and fall-prone elderly. Changes in the size and asymmetry of the basin will be correlated with age and disease state. For instance, a healthy individual may be able to lean evenly in all direction, while a fall-prone individual may only be able to lean well in specific directions.

As opposed to the current qualitative measures, it is hoped that these (and additional) nonlinear measures will differentiate between and definitively classify different patient populations and yield the best set of parameters to create a comprehensive fall risk assessment for clinical use.

The authors would like to thank M.S. Zakynthinaki for kindly sharing her code and sample data and Tim Sauer for helpful discussions. While working on this project, V.A. Smith was funded by the NSF Louis Stokes Alliance for Minority Participation (LSAMP) Fellowship program.

References

1. M.E. Tinetti, N. Engl. J. Med. **348**, 42 (2003)
2. CDC Web-based Injury Statistics Query and Reporting System (WISQARS), 2015, http://www.cdc.gov/injury/wisqars/
3. J. Milat, W.L. Watson, et al., NSW Public Health Bull. **22**, 43 (2011)
4. D. Cameron, G.R. Murray, et al., Cochrane Database Syst. Rev. CD005465 (2010)
5. J.J. Collins, C.J. De Luca, Exp. Brain Res. **95**, 308 (1993)
6. M. Pondal, T. Del Ser, J. Geriatr. Phys. Ther. **31**, 57 (2008)
7. M. Mancini, F.B. Horak, Eur. J. Phys. Rehabil. Med. **46**, 239 (2010)
8. T.E. Lockhart, J. Liu, Ergonomics **51**, 1860 2008
9. R. Armiyoon, C.Q. Wu, Nonlinear Dyn. **79**, 275 (2014)
10. A. Priplata, J. Niemi, et al., Phys. Rev. Lett. **89**, 238101 (2002)
11. P.C. Fino, A.R. Mojdehi, et al., Ann. Biomed. Eng. **44**, 1636 2015
12. F.G. Borg, G. Laxåback, J. Neuroeng. Rehabil. **7**, 38 (2010)
13. R. Soangra, T.E. Lockhart, Biomed. Sci. Instrum. **49**, 180 (2013)
14. L.K. Boulgarides, S.M. McGinty, J.A. Willett, C.W. Barnes, Phys. Ther. **83**, 328 (2003)
15. J.A. Norris, A.P. Marsh, I.J. Smith, R.I. Kohut, M.E. Miller, J. Biomech. **38**, 1263 2005
16. P.B. Thapa, P. Gideon, et al., J. Gerontol. A: Biol. Sci. Med. Sci. **51**, M239 (1996)
17. M. Piirtola, P. Era, Gerontology **52**, 1 (2006)
18. J.R. Stirling, M.S. Zakynthinaki, Chaos **14**, 96 (2004)
19. M.S. Zakynthinaki, J. Stirling, et al., Chaos **20**, 013119 (2010)
20. J. O'Rourke, *Computational Geometry in C* (Cambridge University Press, Cambridge, UK, 1998)
21. R.L. Graham, Inf. Process. Lett. **1**, 132 (1972)
22. T.M. Chan, Discr. Comput. Geom. **16**, 361 (1996)
23. G. Almkvist, B. Berndt, Am. Math. Monthly **95**, 585 (1988)
24. T.M. Owings, M.J. Pavol, K.T. Foley, M.D. Grabiner, J. Am. Geriatr. Soc. **48**, 42 (2000)
25. H.B. Menz, M.E. Morris, S.R. Lord, J. Gerontol. A: Biol. **60**, 1546 (2005)
26. T. Sauer, Physica D **58**, 193 (1992)
27. P.G. Vaidya, P.S. SajiniAnand, N. Nagaraj, Acta Appl. Math. **112**, 205 (2010)